NANO · MICRO small
www.small-journal.com

Deep Blue Emitting Lead Halide Perovskite and Metal-Organic Framework Glass Composites Through Mechanochemistry

*Wupeng Wang, Milton Chai, Wengang Huang, Zixi Xie, Mehri Ghasemi, Prabal Dweep Khanikar, Fangfang Yuan, Kaijie Xu, Yuelei Chen, Xiaoming Wen, Pengfei Qi, Junyong Zhu, Ebinazar B. Namdas, Vicki Chen, Anthony K Cheetham, Lianzhou Wang, and Jingwei Hou**

Mixed-halide perovskites are promising materials for optoelectronic applications due to their tunable bandgaps and high photoluminescence quantum yields. However, these materials face challenges such as phase segregation under excitation and instability when exposed to polar solvents, especially in blue-emitting regions. In this study, a facile mechanochemical synthesis method is developed to produce $CsPb(Br_xCl_{1-x})_3$ - MOF (Metal-organic framework) glass composites. By precisely controlling the halide composition and optimizing milling conditions, glass composites containing quantum-confined perovskite particles with significantly improved phase stability, photoluminescence (PL), and solvent resistance are achieved. Notably, the composite can maintain up to 77% PL efficiency after soaking in water for a year. Structural and optical analyses revealed that the mechanochemical process fosters interfacial bonding between the perovskite and MOF glass, effectively regulating perovskite particle size and passivating surface defects. To demonstrate practical applications, violet and blue light-emitting diode (LED) devices are fabricated, achieving CIE color coordinates of (0.152, 0.031) and (0.134, 0.045), respectively. This work offers a scalable, eco-friendly approach to synthesizing stable, high-performance blue-emitting perovskites, paving the way for their integration into next-generation optoelectronic devices.

1. Introduction

Cesium lead halide perovskites ($CsPbX_3$, X = Cl, Br and I) have gained significant attention in recent years for their potential in high-performance lighting and display technologies. Known for their bright, narrow-band photoluminescence, these materials exhibit tunable emission across the visible spectrum by varying the compositions of halides.[1] However, stability challenges have hindered the practical application of cesium lead halide perovskites. Due to their ionic nature and low formation energy, these materials are thermodynamically and chemically unstable.[2] This instability leads to significant decomposition when exposed to polar solvents, light, heat, and oxygen, limiting their potential applications. These situations are even worse for blue and violet light emitting perovskite due to their larger bandgap, higher excitation binding energy, unstable mixing halide structure (Cl/Br) and more sever lattice strain of Cl and Br.[3] Additionally,

W. Wang, M. Chai, W. Huang, Z. Xie, K. Xu, Y. Chen, L. Wang, J. Hou
School of Chemical Engineering
The University of Queensland
St Lucia, QLD 4072, Australia
E-mail: jingwei.hou@uq.edu.au

The ORCID identification number(s) for the author(s) of this article can be found under https://doi.org/10.1002/smll.202411484

DOI: 10.1002/smll.202411484

M. Ghasemi, X. Wen
Centre for Atomaterials and Nanomanufacturing
RMIT University
Melbourne, VIC 3000, Australia

P. D. Khanikar, E. B. Namdas
School of Mathematics and Physics
University of Queensland
St Lucia, QLD 4072, Australia

F. Yuan
School of Mechanical & Mining Engineering
University of Queensland
St Lucia, QLD 4072, Australia

V. Chen
University of Technology Sydney
Broadway, NSW 2007, Australia

successful application of perovskites requires overcoming other inherent issues, including polymorphism, trap states, the leaching of toxic lead ions and phase segregation for the mixed halide materials.[4]

In the pursuit of stabilizing cesium lead halide perovskites, researchers have explored a range of composite materials, including polymers, inorganic nanoparticles and glasses, each offering unique stabilization mechanisms.[5] Polymers provide flexibility and easy processability, creating encapsulating layers that protect perovskites from moisture and oxygen degradation. Inorganic glasses, often highly stable and inert, offer excellent thermal and chemical stability and have been shown to encapsulate perovskite nanocrystals effectively, reducing their sensitivity to environmental conditions. Similarly, inorganic nanoparticles serve as rigid, protective hosts, enabling a barrier effect that prevents decomposition under exposure to light and heat.[6] However, while these composites enhance stability, maintaining high photoluminescence (PL), particularly in the blue emission region, remains particularly challenging. This spectral range is prone to phase segregation and defect formation, which can lead to a rapid decline in optical performance. Thus, achieving an optimal composite structure that balances stability with high PL efficiency, particularly in the deep blue and violet regions, continues to be a primary goal in perovskite research, which is essential for their practical application in display and lighting technologies.

Forming hybrid glass-perovskite composites presents a promising solution to the issues mentioned above. Among various hybrid glasses, metal-organic framework glasses—compounds consisting of metal ions or clusters coordinated with organic ligands—stand out.[7] Their rich coordination environment and adjustable chemical reactivity offer excellent opportunities for composite formation.[8] In addition, the processability of glass and glass composites makes them an attractive matrix for device fabrication.[9] However, most reported MOF glass-perovskite composites are created through high-temperature liquid phase sintering.[10] While this method effectively forms interfacial bonds, it can lead to thermal decomposition, which may not be suitable for all material types. Therefore, alternative methods for integrating functional materials and MOF glasses are necessary.

A. K Cheetham
Materials Department and Materials Research Laboratory
University of California
Santa Barbara, CA 93106, USA
L. Wang
Nanomaterials Centre
Australian Institute for Bioengineering and Nanotechnology (AIBN)
The University of Queensland
St Lucia, QLD 4072, Australia
P. Qi
College of Materials Science and Engineering
Qingdao University
Qingdao 266071, P. R. China
J. Zhu
School of Chemical Engineering
Zhengzhou University
Qingdao University
Zhengzhou 450001, P. R. China

In this study, we introduce a novel approach using a solvent-free mechanochemical method to fabricate hybrid composites, which offers a robust alternative to conventional liquid-phase sintering.[12] Benefits of the process include high scalability and flexibility in controlling the reaction conditions.[13] Through simple ball milling, we successfully composited $CsPbCl_2Br$ and $CsPbCl_{1.5}Br_{1.5}$ with the MOF glass, achieving enhanced stability and bright blue photoluminescence superior to the high-temperature treatments. Detailed structural analysis and insights into interfacial interactions were obtained through an array of advanced techniques, including X-ray total scattering with pair distribution function (PDF) analysis, synchrotron-based THz Far-IR spectroscopy, X-ray absorption near-edge structure (XANES), extended X-ray absorption fine structure (EXAFS), and solid-state nuclear magnetic resonance (SSNMR). These techniques provide a comprehensive understanding of the composite structure and the interfacial mechanisms that enhance stability and performance. This work highlights the potential of mechanochemical synthesis for creating stable perovskite-MOF composites, particularly for applications that demand high blue emission photoluminescence and resistance to degradation. The mechanochemical process promotes controlled interfacial interactions, resulting in robust materials that withstand high-power laser excitation and prolonged exposure to polar solvents. We believe these findings contribute valuable insights into mechanochemistry, MOF glass stabilization, and the development of durable perovskite-based photonic materials.

2. Results and Discussion

2.1. Fabrication of Composites via Mechanochemistry

The perovskite MOF glass composites were fabricated with two types of precursors: 25 wt.% mixed halide cesium lead perovskites ($CsPbCl_2Br$ or $CsPbCl_{1.5}Br_{1.5}$), synthesized directly from stoichiometric precursors using a mechanochemical process, and 75 wt.% a_gZIF-62 [$Zn(imidazolate)_{1.95}(benzimidazolate)_{0.05}$], where "$a_g$" denotes amorphization by glass transition. The precursors were placed into a ball milling jar and subjected to mechanochemical treatment for varying durations (up to 120 min). The resultant samples were denoted as $(CsPbCl_2Br)_{0.25}(a_g\text{ZIF-62})_{0.75}$ or $(CsPbC_{1.5}Br_{1.5})_{0.25}(a_g\text{ZIF-62})_{0.75}$. Detailed procedures were listed in the Supplementary Information. In this work, a relatively low ratio of the benzimidazolate versus imidazolate ligand was implemented [$Zn(imidazolate)_{1.95}(benzimidazolate)_{0.05}$, ZIF-62] to reduce the melting temperature of the glass phase and therefore improve the flowing capability of ZIF-62 glass.[14] The composite fabricated using crystalline ZIF-62 was also implemented as a comparison.

According to the X-ray powder diffraction (XRD) data (**Figure 1a**; Figures S1 and S2, Supporting Information), the mixed halide perovskite precursors ($CsPbCl_2Br$) exhibited a relatively high crystallinity. The peak positions aligned well with the expected XRD patterns of perovskites as reported in the literature.[11] For the $(CsPbCl_2Br)_{0.25}(a_g\text{ZIF-62})_{0.75}$ composites, the board peak centered at ≈16° could be attributed to the amorphous a_gZIF-62 phase (Figure S1, Supporting Information).The diffraction patterns from the

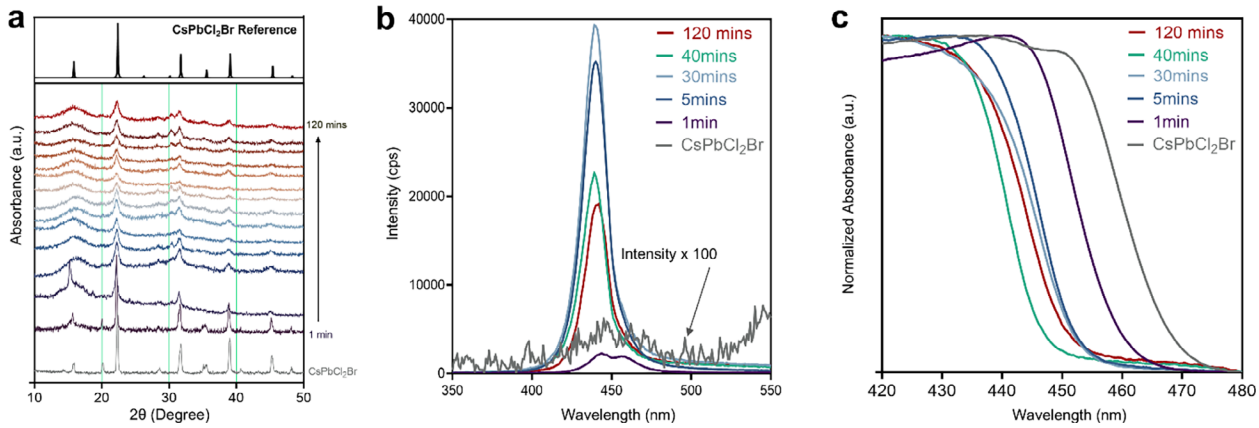

Figure 1. a) Ex situ X-ray diffraction of $(CsPbCl_2Br)_{0.25}(a_gZIF\text{-}62)_{0.75}$ from 1 min to 120 min milling, with perovskite reference pattern.[11] b) PL spectra of $(CsPbCl_2Br)_{0.25}(a_gZIF\text{-}62)_{0.75}$ under different milling time. The pure $CsPbCl_2Br$ was used as a reference. c) Normalized UV-VIS absorbance spectra of $(CsPbCl_2Br)_{0.25}(a_gZIF\text{-}62)_{0.75}$.

perovskite phase were effectively preserved after compositing, though a gradual broadening was observed following extended milling. This could be attributed to either partial amorphization or size reduction for the crystalline perovskite grains. For comparison, we also performed identical milling on pure perovskites (Figure S2, Supporting Information) and the results did not show significant peak broadening nor the loss of crystallinity, despite a much higher mechanical stress being directly applied to the materials. It has been reported that the Cl and Br mixed halide perovskite featured a stable perovskite phase at ambient conditions, and these thermodynamically favorable phases are highly resistant to mechanical amorphization.[15] Therefore, the peak broadening should be associated with the interfacial interactions between the perovskite and MOF glass phases during the mechanochemical process. A similar trend was also observed in the results of $(CsPbCl_{1.5}Br_{1.5})_{0.25}(a_gZIF\text{-}62)_{0.75}$ composites (Figure S3a, Supporting Information).

2.2. Photophysics of the Composites

Photoluminescence (PL) spectra was gathered on pure perovskite, a_gZIF-62 and composite samples to elucidate their photophysical properties (Figure 1b; Figures S3b–S7, Supporting Information).[16] The emission of pure perovskite was barely detectable, which was not unexpected given the presence of a large density of defects originating from the mechanochemical synthesis process. The composites, in comparison, displayed significant enhancement in the PL intensity after the ball milling. Perovskite to glass ratios were investigated, and 25% perovskite loading showed the strongest PL emission (Figure S4, Supporting Information). For $(CsPbCl_2Br)_{0.25}(a_gZIF\text{-}62)_{0.75}$, the samples began to exhibit noticeable blue emission after just 1 min of mechanochemical compositing, but with a certain degree of halide phase segregation. Prolonging the milling time further enhanced the PL intensity, peaking after ≈30 min of treatment. The undesirable phase segregation was also suppressed. In addition, the mechanochemical treatment could lead to a slight blueshift in the PL peak, which was in agreement with the UV–vis spectra in Figure 1c, indicating a possible quantum confinement effect originated from milling perovskites with MOF glass. The pronounced blueshift in UV–vis spectra with prolonged milling time directly corresponds to bandgap widening driven by quantum confinement effects. This spectral shift is significantly more prominent than the blueshift observed in the photoluminescence (PL) emission spectra of the same samples. The attenuated shift in PL spectra likely stems from the interplay of additional factors—such as defect-state interactions, exciton recombination dynamics, and competing non-radiative pathways—that collectively influence emission behavior beyond the primary bandgap modulation.[17] It should be noted that using crystalline ZIF-62, instead of the glassy a_gZIF-62, for the compositing led to a much weaker PL (Figure S5, Supporting Information). It was expected that the higher entropy state (energy) and flowing capability of the glass phase can offer more advantages over the crystalline counterparts for compositing, leading to enhanced interfacial contacting and interactions.[18] For the pure perovskites, no clear enhancement of the PL was detected subject to the same mechanochemical treatment. Notably, undesirable halide phase segregation became more severe under prolonged milling duration for the pure materials (Figure S7, Supporting Information).

The trend in PL could be further substantiated by PL quantum yield measurement (PLQY, Tables S1 and S2, Supporting Information). For $(CsPbCl_2Br)_{0.25}(a_gZIF\text{-}62)_{0.75}$, PLQY increased from 3.6% (1 min) to 19.2% (30 min), and then decreased to ≈11.8% after 120 min milling. Similarly, for $(CsPbCl_{1.5}Br_{1.5})_{0.25}(a_gZIF\text{-}62)_{0.75}$, PLQY increased from 6.1% (1 min) to 37.3% (20 min) and then dropped back to 29.2% (120 min). It should be noted that these PLQY values were significantly higher than the composites fabricated through liquid phase sintering and were also higher than the reported bulk blue emission perovskite composites.[10b,19] Table S3 (Supporting Information) provides a summary of comparable mixed halide perovskites exhibiting emission peaks in the deep blue and violet regions (PL emission below 480 nm). Unlike many studies that focused on well-protected films, the powder composites fabricated in this work enable the processing into different shapes or coating onto various substrates.[20] These PLQY results, achieved using a simple and solvent-free mechanochemical method, represented a

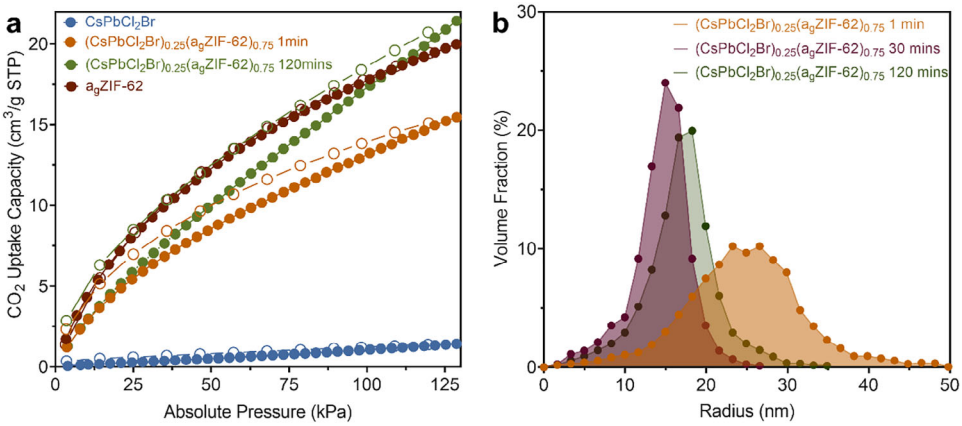

Figure 2. a) CO_2 gas adsorption (Fill) /desorption (No Fill) isotherm of $CsPbCl_2Br$, a_gZIF-62 and $(CsPbCl_2Br)_{0.25}(a_g\text{ZIF-62})_{0.75}$. b) Particle size evolution for $(CsPbCl_2Br)_{0.25}(a_g\text{ZIF-62})_{0.75}$ under different milling time, deconvoluted from the Synchrotron SAXS patterns.

significant advancement in bulk blue and violet perovskite composites and devices.

2.3. Composite Structures

A range of gas adsorption/desorption isotherm tests were performed to understand the effects of ball milling on the composite microporous structure (**Figure 2a**). $CsPbCl_2Br$ is not porous and matches the low gas intake in the adsorption result. When forming $(CsPbCl_2Br)_{0.25}(a_g\text{ZIF-62})_{0.75}$ composites, a_gZIF-62 introduces porosity, and the CO_2 absorption increased with extended mechanochemical milling time. This contrasted with most existing studies where ball milling could lead to porous framework collapse and reduced porosity.[21] The results in this work indicated that ball milling of the two materials could rearrange the coordination bonds within the microporous glassy phase, introducing higher porosity with more tortuous transport pathways, as evidenced by the stronger hysteresis effect. At the same time, due to the relatively small pores of ZIF-62 glass, large gas molecules, for example N_2, were hard to go through and hence showed quite a low gas uptake (Figure S8, Supporting Information)

Differential scanning calorimetry (DSC) provided information on phase transition, thermodynamics and structural relaxation. DSC of pure a_gZIF-62 only featured the second-order phase transition (glass transition T_g) at ≈287.3 °C (Figure S9, Supporting Information). Up on the milling of the pure glass, the T_g experienced a constant decrease from 287.3 to 256.7 °C (after 120 min milling). This observation suggested that energy offered through milling could effectively rearrange the metal-organic coordination bonds, thereby enhancing the internal energy of the ZIF glass phase, beneficial for compositing with the other secondary materials. Up on forming the composite through milling, a similar reduction of the T_g was observed (Figures S10 and S11, Supporting Information) along with higher milling time, indicating the enhanced entropy terms, possibly from the formation of interfacial bonds.

One challenge associated with the mechanochemical process was achieving a high level of homogeneity of the fabricated samples. This was particularly important for the mixed halide perovskites as the phase segregation could readily lead to the PL peak shift and emission quenching.[10a] In this work, the gradually reduced PL full-widths at half-maximum (FWHM) with extended milling indicated the compositing leads to a high level of perovskite homogeneity and a reduction in defect density (Figure S12, Supporting Information). Specifically, FWHM of $(CsPbCl_2Br)_{0.25}(a_g\text{ZIF-62})_{0.75}$ was changed from 32.7 at 1 min milling to ≈19 nm at 2 h milling. It is noteworthy that the mechanochemical process typically resulted in increased defect density.[12,13] However, our findings suggested otherwise, where the glassy MOF could stabilize perovskites and reduce the surface trap states during the high energy milling. Both high-resolution transmission microscopy (TEM) and scanning electron microscopy (SEM) were also implemented to study the surface morphology and phase distribution (Figures S13–S16, Supporting Information). Extending the ball milling time led to a smoother and more continuous surface. Additionally, according to energy-dispersive X-ray spectroscopy (STEM-EDS) elemental distribution mapping in Figures S17–S19 (Supporting Information), Zn, Cs, Pb, Cl and Br were evenly distributed across the examined region after only 1 min mechanochemical compositing. Information about the particle size distribution of the perovskite phase (the main scattering phase) can be retrieved via the synchrotron X-ray small angle scattering (SAXS) on $(CsPbCl_2Br)_{0.25}(a_g\text{ZIF-62})_{0.75}$ (Figure 2b; Figure S20, Supporting Information). With the milling time increase, we could clearly observe size reduction and narrower size distribution of perovskite phase within the fabricated composites, consistent with TEM (Figures S13 and S14, Supporting Information). The particle size within the composite confirms the quantum confinement effect, contributing to the observed blue shift in PL emission and gradual broadening of the XRD peaks.

2.4. Interfacial Properties within the Composites

Despite the metal halide perovskite being reported to have a high tolerance toward bulk and surface defects, the results in this work suggested their performance within the composite was

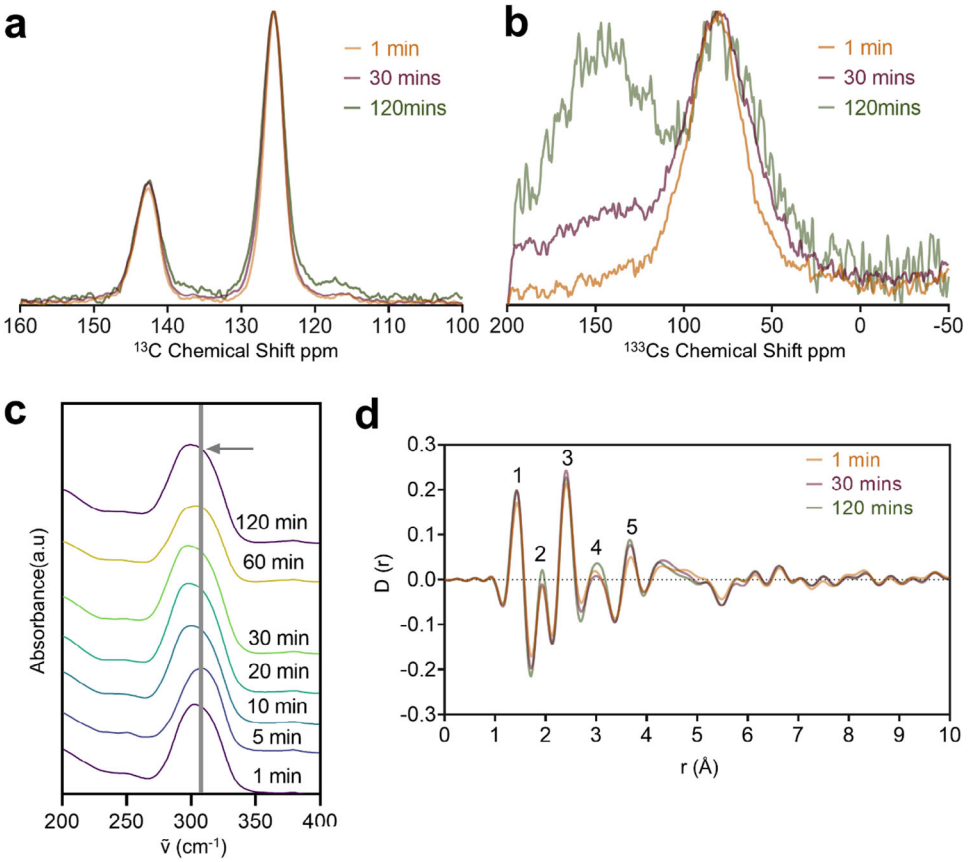

Figure 3. a,b) ^{13}C and ^{133}Cs Solid state nuclear magnetic resonance (SSNMR) of $(CsPbCl_2Br)_{0.25}(a_gZIF\text{-}62)_{0.75}$ under different compositing time. c) Zoom in THz-FarIR spectra of $(CsPbCl_2Br)_{0.25}(a_gZIF\text{-}62)_{0.75}$ under different compositing times. d) Atomic pair distribution function of $(CsPbCl_2Br)_{0.25}(a_gZIF\text{-}62)_{0.75}$ under different compositing times.

highly related to the properties at the interface. Solid state nuclear magnetic resonance (SSNMR) served as a useful complement to vibrational spectroscopy in interfacial bonding studies, as it could provide insights into the element-specific chemical environments. The broader peaks along with ball milling observed in ^{13}C NMR and ^{1}H spectroscopy indicated more structure disorder during composite formation (**Figure 3a**; Figure S21 and S22, Supporting Information). Further analysis of the ^{133}Cs spectra revealed the evolution of the perovskite structure (Figure 3b). The widening of the peak centered at ≈80 ppm suggested an alteration of the pristine Cs environment within the perovskite, which aligned with the reduction of particle size and the enhanced interfacial bonding. A more significant variation occurred in the ^{133}Cs spectra, where the shoulder peak at ≈150 ppm became more prominent after milling. In our previous study, we have investigated the formation of interfacial bonds through high-temperature liquid phase sintering in depth, where the molten MOF liquid could partially dissolve $CsPbI_3$, forming a diffusion alloying layer with Pb-halide octahedra structures.[10a] This results in the formation of a Cs-imidazolate link at the interface, as represented by a shoulder peak at ≈150 ppm region adjacent to the main Cs peak for $CsPbI_3$ at ≈175 ppm. Similar features were also identified in this work, indicating the formation of interfacial Cs imidazolate bonds through external mechanochemical force.

Synchrotron terahertz (THz)/Far-IR spectra utilizes far-IR radiation in the millimeter wavelength range or terahertz frequency region to analyze samples, proving instrumental in determining the spectra of dynamic vibrational motions of metal-organic bonding.[22] In this work, ex situ THz Far-IR spectra were collected on the composite samples with different milling times. Results suggested coherent variations in the original bonding environment following extended compositing (Figure 3c; Figures S23a and S24a, Supporting Information). For the pristine ZIF-62 glass, a peak at ≈300 cm^{-1} could be assigned to Zn-N stretching within the Zn-imidazolate tetrahedra.[22a,c] In the case of $(CsPbCl_2Br)_{0.25}(a_gZIF\text{-}62)_{0.75}$, the feature shifted to a lower wavenumber with increased milling time, suggesting that the original Zn-imidazolate dynamic behavior was altered by new Zn-halide interfacial bonding between the perovskites and MOF glass.[10] Similar interfacial interaction could also be observed in the $(CsPbCl_{1.5}Br_{1.5})_{0.25}(a_gZIF\text{-}62)$ from Figures S23b and S24b (Supporting Information) and the variation of bonding environment for Cs, Zn, N, Pb, Cl and Br was further confirmed by X-ray photoelectron spectroscopy (XPS) in Figures S25–S27 (Supporting Information).

Additionally, pair distribution functions (PDFs), obtained through Fourier transform of the synchrotron X-ray total scattering patterns, could reveal the short to mid-range structure of

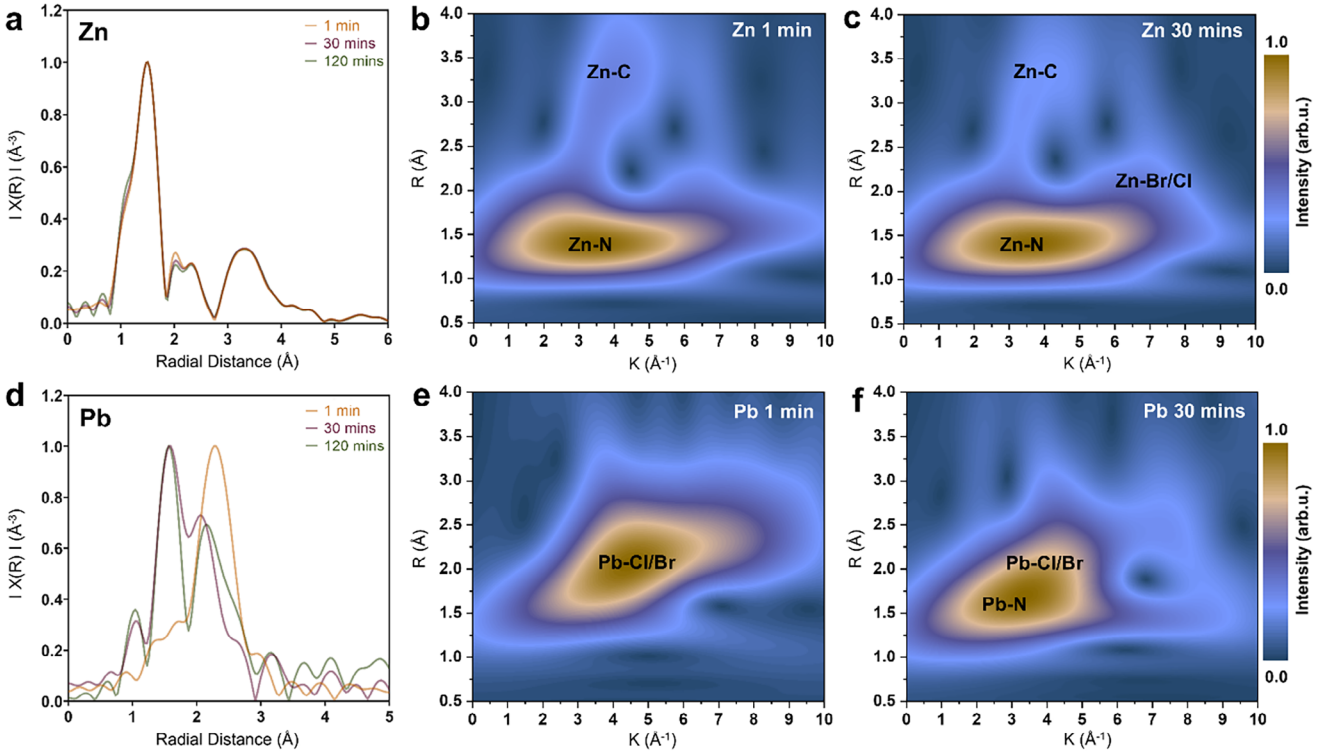

Figure 4. a) Extended X-ray absorption fine structure (EXAFS) Zn K edge spectra of $(CsPbCl_2Br)_{0.25}(a_gZIF\text{-}62)_{0.75}$ under different milling time. b,c) Zn spectra full-range wavelet transform (WT) representation for $(CsPbCl_2Br)_{0.25}(a_gZIF\text{-}62)_{0.75}$ under 1 and 30 min milling. d) Extended X-ray absorption fine structure (EXAFS) Pb L3 edge spectra of $(CsPbCl_2Br)_{0.25}(a_gZIF\text{-}62)_{0.75}$ under different milling time. e,f) Pb spectra full-range wavelet transform (WT) representation for $(CsPbCl_2Br)_{0.25}(a_gZIF\text{-}62)_{0.75}$ under 1 and 30 min milling.

the composite (Figure 3d; Figure S28, Supporting Information). PDFs provide information about the distribution of distances between pairs of different atoms within composites.[23] Peak 1 at ≈1.48 Å was attributed to C—C and C—N pairs originated from organic linkers in ZIF glass; peak 2 (≈2 Å) represented the metal-organic bonds (Zn—N) bonding in ZIF framework.[24] After ball milling, the most significant changes were observed ≈3.0 Å (peak 4), corresponding to lead halide atom pairs within the perovskite phase and Zn—C within the glassy phase, and ≈3.8 Å, corresponding to Cs halide pairs.[10a] These observations were consistent with the formation of interfacial bonds.

To further investigate the bonding environment of Zn and Pb during mechanochemical compositing, and analyze the short-range structure of glassy composites, near edge (XANES) and extended (EXAFS) X-ray absorption fine structure analysis of Zn and Pb were performed (**Figure 4**). XANES results in Figure S29 (Supporting Information) indicate the oxidation state of Zn in $(CsPbCl_2Br)_{0.25}(a_gZIF\text{-}62)_{0.75}$ initially decreases and then increases during the milling process, as indicated by the slight shift of XANES spectra.[25] This observation supported the interfacial bonding rearrangement between Zn-N and Zn-halide bonding during mechanochemical milling.[26] The Zn-EXAFS in Figure 4a revealed that all composites exhibited dominant Zn-N peaks at 1.5 Å, attributed to the pristine Zn—N bonding in MOFs.[27] Following the mechanochemical compositing process, peak alteration between 2 Å and 2.5 Å could be assigned to the newly formed Zn—Br and Zn—Cl bonding.[28] These results aligned with the observation in (THz)/Far-IR spectra and wavelet transforms (WTs) of Zn (Figure 4b,c; Figure S30, Supporting Information). Changes in Pb bonding environment were more significant: in EXAFS and WT results of Pb, 1 min milling composites had the main features being assigned to the Pb-Cl/Br bonding at ≈2.3 Å (Figure 4d–f; Figure S31 and S32, Supporting Information). During mechanochemical milling, the emergence of new peaks below 2 Å could be assigned to newly formed Pb-O bonding (1.7 Å) and Pb-N bonding (1.4 Å).[10a] The occurrence of Pb-O bonding could be attributed to oxidation during high-energy mechanochemical milling, while the Pb-N pairs resulted from coordination between Pb and imidazolate sites during the mechanochemically induced rearrangement of Zn-N bonding within the glassy phase.[24]

2.5. Practical Considerations

The characterization results confirmed that the mechanochemical process effectively generated interfacial bonding between MOF glass and perovskite crystals, resulting in quantum-confined nanocrystals with sufficient surface defect passivation, thereby enhancing PL performance. The fabricated composite materials exhibited excellent stability even in their powder form, as the hydrophobic and rigid glass matrix, along with the interfacial interactions, played a crucial role in protecting the sensitive perovskite component under various conditions, including

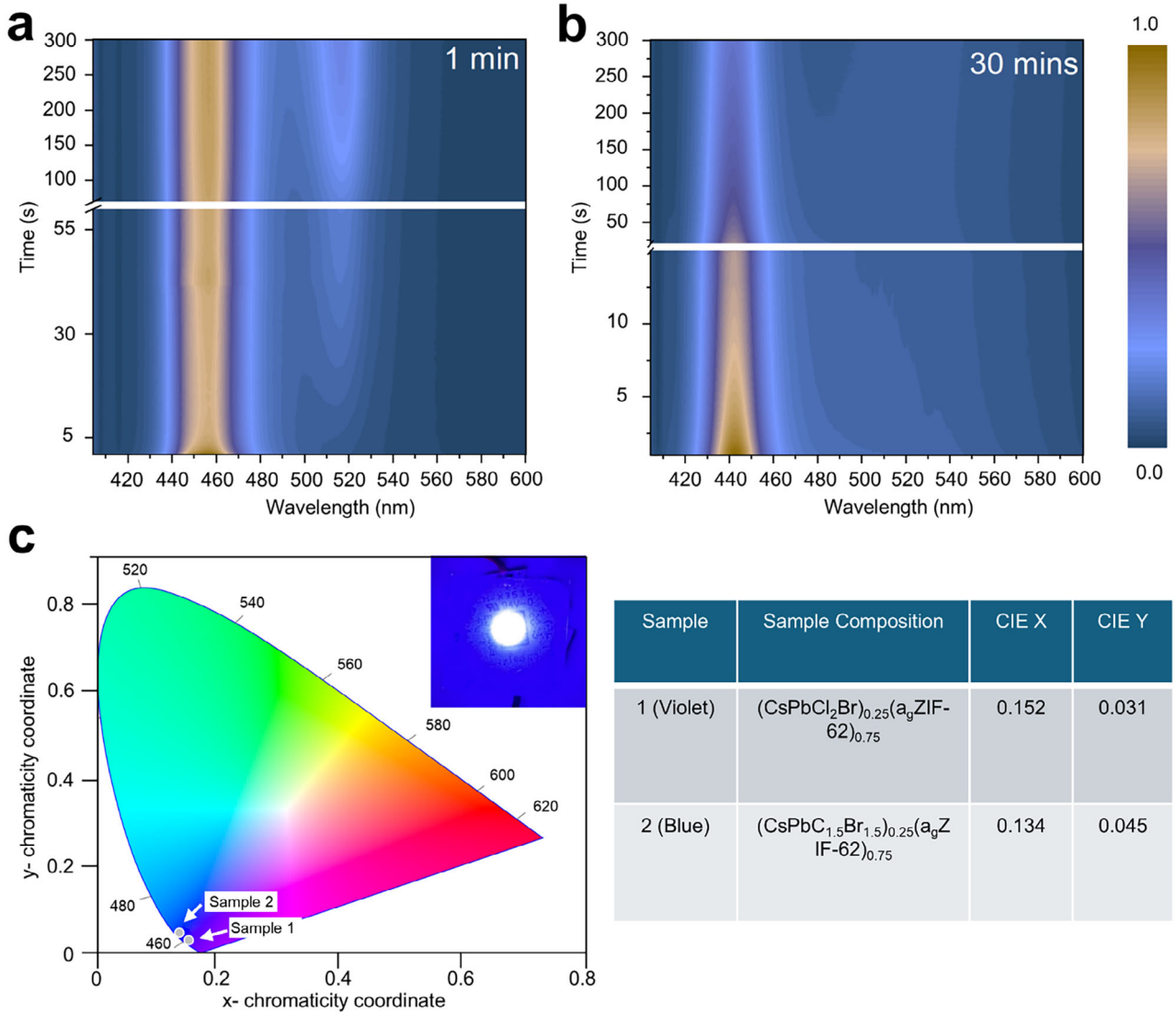

Sample	Sample Composition	CIE X	CIE Y
1 (Violet)	$(CsPbCl_2Br)_{0.25}(a_gZIF\text{-}62)_{0.75}$	0.152	0.031
2 (Blue)	$(CsPbC_{1.5}Br_{1.5})_{0.25}(a_gZIF\text{-}62)_{0.75}$	0.134	0.045

Figure 5. Photoluminescence stability of a) $(CsPbCl_2Br)_{0.25}(a_gZIF\text{-}62)_{0.75}$ 1 min under 500 mW cm^{-2} laser intensity. b) $(CsPbCl_2Br)_{0.25}(a_gZIF\text{-}62)_{0.75}$ 30 min under 500 mW cm^{-2} laser intensity. c) CIE ordinations of fabricated blue and violet LED samples with photo of fabricated LED samples on the top right. Samples were excited with 365 nm commercial LED chips.

exposure to polar solvents and laser irradiation. Remarkably, stable PL emissions were observed for composites after enduring rigorous conditions, such as over 1 year of soaking in water and ethanol, storage under ambient conditions for over 500 days, exposure to continuous laser excitation (500 mW cm^{-2}) for over 300 s, see **Figure 5**a,b and Figures S33–S37 (Supporting Information). It should be noted that soaking in polar solvent can lead to almost immediate decomposition of pure perovskites, whereas the composite still maintained ≈77% and 35% of the PL intensity after 1 year of soaking in water and ethanol, respectively. ICP-OES analysis further indicated that the lead concentration in the soaking solutions was only 0.058 ppm for water and 0.055 ppm for ethanol, corresponding to less than 0.003 wt.% Pb decomposition of 20 mg composites pellets. Additionally, the highly undesirable phase separation could also be effectively mitigated through milling.

Regarding the practicality for device utilization, the mechanochemically synthesized composites in their fine powder form could be readily coated using various coating techniques, including the direct mechanochemical coating we reported previously.[20] Our mechanochemically synthesized devices exhibit robust blue and violet light emission, with the fabricated PeLEDs aligning with the chromaticity coordinates of the RGB primaries as defined in Rec. 2020 (Figure 5c; Figure S38, Supporting Information).[29]

3. Conclusion

In this study, we have demonstrated the effective use of mechanochemical compositing to create stable blue and violet light-emitting $CsPbCl_2Br$ and $CsPbCl_{1.5}Br_{1.5}$ composites with ZIF-62 glass. Our findings reveal that the mechanochemical

approach not only enhances photoluminescence but also mitigates the common stability issues faced by cesium lead halide perovskites, particularly in the challenging blue-violet spectral range. This advancement arises from the formation of strong interfacial bonds between the perovskite and ZIF-62 glass components, which confine exciton recombination, enhance overall stability, and reduce surface trap states. The optimal PL performance results from a well-balanced composite configuration, influenced by factors such as size reduction, heat-induced aggregation, quantum confinement, interfacial bonding, and morphology. However, extended milling time increases the formation of amorphous perovskites, particularly at interfaces, creating additional defect sites that enhance non-radiative recombination and ultimately reduce PL efficiency.[30]

Detailed characterization through X-ray diffraction, NMR, and synchrotron-based spectroscopies confirmed the role of interfacial interactions in enhancing photoluminescence and preventing halide phase segregation. Mechanochemical milling yielded a composite structure with a well-dispersed perovskite phase, enabling resistance to degradation under polar solvents and light. Our findings indicate that these interfacial bonds, along with the protective properties of ZIF-62 glass, contribute significantly to the prolonged stability of the composites, retaining up to 77% PL after one year of water immersion in the powder form.

The potential applications of these composites extend to various LED technologies due to their flexible, powder-based form and compatibility with different substrate coating techniques. By achieving stable violet and blue emissions that align closely with the Rec. 2020 color gamut, this work marks an important step toward practical, stable, and efficient lighting materials.

Overall, this study highlights mechanochemical synthesis as a scalable, solvent-free, and environmentally friendly strategy for fabricating perovskite-MOF glass composites, offering promising pathways for the development of next-generation photonic devices. Additionally, we have reported two types of perovskites with different Br/Cl ratios, and both series showed very similar behavior under mechanochemical treatment. It is reasonable to expect this technology will be applicable to other lead halide perovskite as well.

Supporting Information

Supporting Information is available from the Wiley Online Library or from the author.

Acknowledgements

W.W. would like to thank the Australian government and the University of Queensland for the Graduation School Scholarship support. J.H. acknowledges the financial support from the Australian Research Council (FT210100589 and DP230101901) and the Australian Economy Accelerator Grant (AE230200076). V.C. acknowledges the financial support from the Australian Research Council (DP230103192).

Open access publishing facilitated by The University of Queensland, as part of the Wiley - The University of Queensland agreement via the Council of Australian University Librarians.

Conflict of Interest

The authors declare no conflict of interest.

Data Availability Statement

The data that support the findings of this study are available from the corresponding author upon reasonable request.

Keywords

blue-violet light LEDs, composites, mechanochemistry, MOF glass, perovskites

Received: November 28, 2024
Revised: March 3, 2025
Published online: April 7, 2025

[1] H. Huang, M. I. Bodnarchuk, S. V. Kershaw, M. V. Kovalenko, A. L. Rogach, *ACS Energy Lett.* **2017**, *2*, 2071.

[2] a) J. A. Steele, H. Jin, I. Dovgaliuk, R. F. Berger, T. Braeckevelt, H. Yuan, C. Martin, E. Solano, K. Lejaeghere, S. M. J. Rogge, C. Notebaert, W. Vandezande, K. P. F. Janssen, B. Goderis, E. Debroye, Y.-K. Wang, Y. Dong, D. Ma, M. Saidaminov, H. Tan, Z. Lu, V. Dyadkin, D. Chernyshov, V. Van Speybroeck, E. H. Sargent, J. Hofkens, M. B. J. Roeffaers, *Science* **2019**, *365*, 679; b) Y. Zhao, C. Xie, X. Zhang, P. Yang, *ACS Appl. Nano Mater.* **2021**, *4*, 5478.

[3] a) X. Yang, L. Ma, M. Yu, H.-H. Chen, Y. Ji, A. Hu, Q. Zhong, X. Jia, Y. Wang, Y. Zhang, R. Zhu, X. Wang, C. Lu, *Light: Sci. Appl.* **2023**, *12*, 177; b) D. Hong, P. Zhao, Y. Du, C. Zhao, Y. Xia, Z. Wei, Z. Jin, Y. Tian, *iScience* **2020**, *23*, 101415; c) A. J. Knight, J. Borchert, R. D. J. Oliver, J. B. Patel, P. G. Radaelli, H. J. Snaith, M. B. Johnston, L. M. Herz, *ACS Energy Lett.* **2021**, *6*, 799; d) B. Yang, D. Bogachuk, J. Suo, L. Wagner, H. Kim, J. Lim, A. Hinsch, G. Boschloo, M. K. Nazeeruddin, A. Hagfeldt, *Chem. Soc. Rev.* **2022**, *51*, 7509.

[4] a) T. A. S. Doherty, A. J. Winchester, S. Macpherson, D. N. Johnstone, V. Pareek, E. M. Tennyson, S. Kosar, F. U. Kosasih, M. Anaya, M. Abdi-Jalebi, Z. Andaji-Garmaroudi, E. L. Wong, J. Madéo, Y.-H. Chiang, J.-S. Park, Y.-K. Jung, C. E. Petoukhoff, G. Divitini, M. K. L. Man, C. Ducati, A. Walsh, P. A. Midgley, K. M. Dani, S. D. Stranks, *Nature* **2020**, *580*, 360; b) S.-Y. Bae, S. Y. Lee, J.-W. Kim, H. N. Umh, J. Jeong, S. Bae, J. Yi, Y. Kim, J. Choi, *Sci. Rep.* **2019**, *9*, 4242.

[5] a) N. Shivaprasad, M. G. Veena, B. S. Madhukar, R. Kavya, K. Sarath, P. R. Vanga, G. S. Dennish Babu, B. Mahesha Sachith, A. V. Raghu, *Inorg. Chem. Commun.* **2024**, *159*, 111761; b) Q. Zeng, X. Zhang, X. Feng, S. Lu, Z. Chen, X. Yong, S. A. T. Redfern, H. Wei, H. Wang, H. Shen, W. Zhang, W. Zheng, H. Zhang, J. S. Tse, B. Yang, *Adv. Mater.* **2018**, *30*, 1705393; c) S. Gull, S. Batool, G. Li, M. Idrees, *Front. in Chem.* **2022**, *10*, 1020484; d) M. Shellaiah, K. W. Sun, N. Thirumalaivasan, M. Bhushan, A. Murugan, *Sensors* **2024**, *24*, 2504.

[6] a) B. H. Alshammari, M. M. A. Lashin, M. A. Mahmood, F. S. Al-Mubaddel, N. Ilyas, N. Rahman, M. Sohail, A. Khan, S. S. Abdullaev, R. Khan, *RSC Advances* **2023**, *13*, 13735; b) X.-L. Huang, *iScience* **2024**, *27*, 109555.

[7] W. Wang, M. Chai, R. Lin, F. Yuan, L. Wang, V. Chen, J. Hou, *Energy Advances* **2023**, *2*, 1591.

[8] J. Hou, C. W. Ashling, S. M. Collins, A. Krajnc, C. Zhou, L. Longley, D. N. Johnstone, P. A. Chater, S. Li, M.-V. Coulet, P. L. Llewellyn, F.-X. Coudert, D. A. Keen, P. A. Midgley, G. Mali, V. Chen, T. D. Bennett, *Nat. Commun.* **2019**, *10*, 2580.

[9] R. Lin, M. Chai, Y. Zhou, V. Chen, T. D. Bennett, J. Hou, *Chem. Soc. Rev.* **2023**, *52*, 4149.

[10] a) X. Li, W. Huang, A. Krajnc, Y. Yang, A. Shukla, J. Lee, M. Ghasemi, I. Martens, B. Chan, D. Appadoo, P. Chen, X. Wen, J. A. Steele, H. G. Hackbarth, Q. Sun, G. Mali, R. Lin, N. M. Bedford, V. Chen, A. K. Cheetham, L. H. G. Tizei, S. M. Collins, L. Wang, J. Hou, *Nat. Com-*

mun. **2023**, *14*, 7612; b) J. Hou, P. Chen, A. Shukla, A. Krajnc, T. Wang, X. Li, R. Doasa, L. H. G. Tizei, B. Chan, D. N. Johnstone, R. Lin, T. U. Schülli, I. Martens, D. Appadoo, M. S. Ari, Z. Wang, T. Wei, S.-C. Lo, M. Lu, S. Li, E. B. Namdas, G. Mali, A. K. Cheetham, S. M. Collins, V. Chen, L. Wang, T. D. Bennett, *Science* **2021**, *374*, 621.

[11] X. He, Y. Qiu, S. Yang, *Adv. Mater.* **2017**, *29*, 1700775.

[12] S. Mateti, M. Mathesh, Z. Liu, T. Tao, T. Ramireddy, A. M. Glushenkov, W. Yang, Y. I. Chen, *Chem. Commun.* **2021**, *57*, 1080.

[13] W. Wang, M. Chai, M. Y. Bin Zulkifli, K. Xu, Y. Chen, L. Wang, V. Chen, J. Hou, *Mol. Syst. Des. Eng.* **2023**, 560.

[14] L. Frentzel-Beyme, M. Kloß, P. Kolodzeiski, R. Pallach, S. Henke, *J. Am. Chem. Soc.* **2019**, *141*, 12362.

[15] a) A. Karmakar, M. S. Dodd, X. Zhang, M. S. Oakley, M. Klobukowski, V. K. Michaelis, *Chem. Commun.* **2019**, *55*, 5079; b) D. Ding, H. Li, J. Li, Z. Li, H. Yao, L. Liu, B. B. Tian, C. Su, F. Chen, Y. Shi, *J. Mater. Chem. A* **2019**, *7*, 540.

[16] R. Gaillac, P. Pullumbi, K. A. Beyer, K. W. Chapman, D. A. Keen, T. D. Bennett, F.-X. Coudert, *Nat. Mater.* **2017**, *16*, 1149.

[17] A. F. Gualdrón-Reyes, *Adv. Opt. Mater.* **2025**, *13*, 2402043.

[18] P. G. Debenedetti, F. H. Stillinger, *Nature* **2001**, *410*, 259.

[19] a) P. Du, J. Li, L. Wang, J. Liu, S. Li, N. Liu, Y. Li, M. Zhang, L. Gao, Y. Ma, J. Tang, *ACS Appl. Mater. Interfaces* **2019**, *11*, 47083; b) F. Yuan, C. Ran, L. Zhang, H. Dong, B. Jiao, X. Hou, J. Li, Z. Wu, *ACS Energy Lett.* **2020**, *5*, 1062; c) M. Karlsson, Z. Yi, S. Reichert, X. Luo, W. Lin, Z. Zhang, C. Bao, R. Zhang, S. Bai, G. Zheng, P. Teng, L. Duan, Y. Lu, K. Zheng, T. Pullerits, C. Deibel, W. Xu, R. Friend, F. Gao, *Nat. Commun.* **2021**, *12*, 361; d) S. Lee, J. Kim, H. Kim, C. Kim, S. Kim, C. Kim, H. Lee, B. Choi, C. Muthu, T. Kim, J. Lee, S. Lee, H. Ihee, J.-Y. Lee, *Sci. Adv.* **2024**, *10*, eadn8465.

[20] R. Lin, Y. Yao, M. Y. B. Zulkifli, X. Li, S. Gao, W. Huang, S. Smart, M. Lyu, L. Wang, V. Chen, J. Hou, *Nanoscale* **2022**, *14*, 2221.

[21] C. Ma, Z. Yang, X. Guo, Z. Qiao, C. Zhong, *J. Membr. Sci.* **2022**, *663*, 121069.

[22] a) A. F. Möslein, J.-C. Tan, *J. Phys. Chem. Lett.* **2022**, *13*, 2838; b) K. Hamilton, J. Neu, *APL Mater.* **2024**, *12*; c) M. R. Ryder, B. Civalleri, T. D. Bennett, S. Henke, S. Rudić, G. Cinque, F. Fernandez-Alonso, J. C. Tan, *Phys. Rev. Lett.* **2014**, *113*, 215502.

[23] S. J. L. Billinge, *Philos. Trans. R. Soc., A* **2019**, *377*, 20180413.

[24] M. F. Thorne, A. F. Sapnik, L. N. McHugh, A. M. Bumstead, C. Castillo-Blas, D. S. Keeble, M. D. Lopez, P. A. Chater, D. A. Keen, T. D. Bennett, *Chem. Commun.* **2021**, *57*, 9272.

[25] A. Tougerti, S. Cristol, E. Berrier, V. Briois, C. La Fontaine, F. Villain, Y. Joly, *Phys. Rev. B* **2012**, *85*, 125136.

[26] a) J. Li, Y. Geng, Z. Xu, P. Zhang, G. Garbarino, M. Miao, Q. Hu, X. Wang, *JACS Au* **2023**, *3*, 402; b) H. Sui, Y. Rong, J. Song, D. Zhang, H. Li, P. Wu, Y. Shen, Y. Huang, *J. Hazard. Mater.* **2018**, *342*, 201.

[27] a) R. Boada, J. Chaboy, S. Hayama, L. L. Keenan, A. A. Freeman, M. Amboage, S. Díaz-Moreno, *J. Phys. Chem. C* **2022**, *126*, 5935; b) X. Wang, W. Hu, X.-H. Xia, C. Wang, *Adv. Funct. Mater.* **2023**, *33*, 2212798.

[28] a) T. Niwa, Y. Uetake, M. Isoda, T. Takimoto, M. Nakaoka, D. Hashizume, H. Sakurai, T. Hosoya, *Nature Catalysis 4*, 1080; b) J. Wong, F. W. Lytle, *J. Non-Cryst. Solids* **1980**, *37*, 273.

[29] K. Masaoka, Y. Nishida, M. Sugawara, *Opt. Express* **2014**, *22*, 19069.

[30] Y. Lei, Y. Chen, S. Xu, *Matter* **2021**, *4*, 2266.